Keshvari, A., Darbari, S., & Taghavi, M. (2018). Self-Powered Plasmonic UV Detector, Based on Reduced Graphene Oxide/Ag Nanoparticles. *IEEE Electron Device Letters*, *39*(9), 1433-1436. [8409391]. https://doi.org/10.1109/LED.2018.2854733

This article has been accepted for publication in a future issue of this journal, but has not been fully edited. Content may change prior to final publication. Citation information: DOI 10.1109/LED.2018.2854733, IEEE Electron Device Letters

# Self-powered plasmonic UV detector, based on reduced graphene oxide/Ag nanoparticles

A. Keshvari, S. Darbari, *Member, IEEE*, M. Taghavi

***Abstract*- We report a plasmonic self-powered UV detector based on triboelectric nanogenerators, for the first time. The proposed structure benefits from plasmon-assisted photoresponse in reduced graphene oxide/Ag nanoparticles heterostructure, serving as a high sensitive photoconductive layer in the fabricated triboelectric nanogenerator. Ag nanoparticles enhance the contacting surface area of the triboelectric nanogenerator, and improve the output open circuit voltage by a factor of about 5. The presented triboelectric nanogenerator operates as an active self-powered UV detector, so that the open circuit voltage is modulated by the UV illumination. The open circuit voltage sensitivity ($\Delta V_{p\text{-}p}/V_{p\text{-}p}$) is measured as about 50 % in response to UV illumination, with illumination power density of 500 µW/cm$^2$.**

**Index Terms:** Triboelectric nanogenerator, plasmon, reduced graphene oxide, Ag nanoparticles, self-powered photodetector;

## I. Introduction

Emergence of the miniature and low-power electronic systems has highlighted the importance of generating the required electric power from environmental energies such as sun light, motions and vibrations. On the other hand, using battery power involves environmentally unfriendly materials, and restricts the lifespan, stability of power, and scalability of the systems. Thus mechanical energy harvesting has attracted massive interests during the last decade. Among various principles for harvesting mechanical energy [1-3], triboelectric nanogenerators (TENGs) have shown promising properties and wide applications [4-11], since their first invention in 2012. TENGs have shown high energy conversion efficiencies [12], low cost fabrication process, and integration potential [13]. In this field of research, self-powered devices and sensors have been proposed as one of the most attractive applications of TENGs [14-17]. However, there are limited reports on self-powered photodetectors based on TENGs [18-20]. Here, for the first time, we propose a plasmonic self-powered UV detector, benefiting from reduced graphene oxide (rGO)/Ag nanoparticles (Ag NPs) heterostructure. The proposed UV detector is a self-powered active sensor that can generate electrical signal as a response to UV-illumination and environmental tapping energies.

## II. Fabrication Process and Operation Principle

First, Ag NPs are synthesized by solution method, in which silver nitrate ($AgNO_3$) is the precursor and sodium borohydride ($NaBH_4$) serves as the reducing agent and stabilizer [21]. Then, graphene oxide (GO) is synthesized by modified Hummer's method [22], from graphite powder. The resultant GO powder is dissolved in DI water and sonicated for 30 minutes. To prepare polydimethylsiloxane (PDMS) layers, silicone elastomer base and the curing agent[1] (Sylgard184 from Dow Corning Company) are mixed at the ratio of 10:1, for 10 minutes. The mixture is degassed from the created bubbles after a 10-minute period of relaxing. Then, the prepared PDMS is spin-coated on a pre-cleaned indium tin oxide (ITO) coated glass, and cured at 100°C for 35 minutes. Fig. 1(a-d) display the fabrication process of the proposed TENG, schematically. The PDMS surface on the ITO electrode (Fig. 1.a) is treated by an oxygen plasma (Fig. 1.b) in order to be rendered hydrophilic, which is necessary for the uniform coating of Ag NPs from its aqua solution. RF plasma power is 50W, oxygen flow rate is 100sccm, and plasma time duration is about 1 minute in this step. Then the prepared solution of Ag NPs is drop casted on the surface of the PDMS layer, and dried at 60°C. This cycle is repeated for six times (Fig. 1.c). Then the synthesized rGO sheets are deposited on the sample by dip coating, and dried (Fig. 1.d). The schematic operation principle of the fabricated TENG in contact/separation mode is illustrated in parts (e-i) of Fig. 1. This operation is based on coupling between electrostatic effect and triboelectric effect. As shown in Fig. 1.e, rGO and steel electrodes are two contacting surfaces in the fabricated TENG. When these two surfaces come into contact, a chemical bond is formed between them and charge injection occurs from metallic electrode to the rGO surface, due to their electrochemical potential difference (Fig. 1.f). Hence, a positive charge is created on steel, while a negative charge is formed on the surface of rGO [23]. When the contacting surfaces are released, some of the bonded atoms keep extra

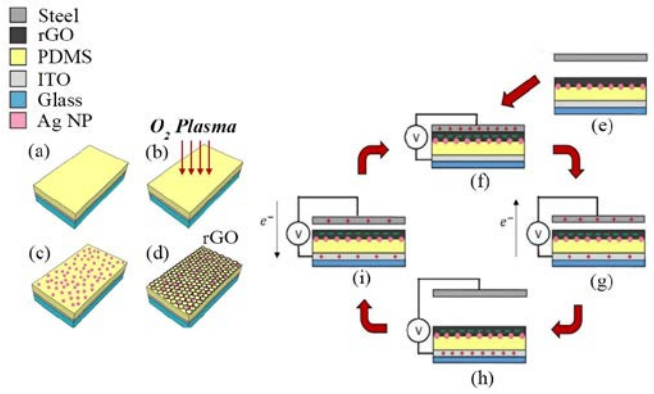


Fig. 1. (a) Coating of PDMS layer on an ITO-coated glass. (b) Oxygen plasma treatment. (c) Deposition of Ag NPs. (d) Dip coating of rGO sheets. (e) Cross section view of the fabricated TENG. (f) Creation of tribo charges on the contacting surfaces. (g) Potential difference is established, causing electrons to flow from ITO to steel plate, during separation. (h) Charges on steel plate are completely screened. (i) Next pressing cycle, when electrons are driven in the opposite direction.

A. Keshvari (arvin.keshvari@gmail.com) and S. Darbari (s.darbari@modares.ac.ir) are both with Nano Sensors and Detectors Lab., and Nano Plasmophotonic Research Group, Faculty of Electrical and Computer Engineering, Tarbiat Modares University, Tehran 1411713116, Iran. M. Taghavi (majid.taghavi@bristol.ac.uk) is with Department of Engineering Mathematics, University of Bristol, Bristol, BS8 1UB, UK.

This article has been accepted for publication in a future issue of this journal, but has not been fully edited. Content may change prior to final publication. Citation information: DOI 10.1109/LED.2018.2854733, IEEE Electron Device Letters

electrons, while some have a tendency to give them away, which is believed to be the reason behind creating tribo charges. After separation, a lower potential is established at the back electrode (ITO). Thus, electrons are driven from the ITO electrode to the steel electrode (Fig. 1.g), until the charges on the steel plate are completely screened (Fig. 1.h). By applying force during the next pressing step, electrons will flow in opposite direction to rebalance the charges (Fig. 1.i). After a complete contact, charges on two surfaces will be equal once again (Fig. 2.f), and the presented cycle be repeated.

## III. Results and Discussions

Fig. 2.a illustrates the TEM image of the synthesized Ag NPs with an average size of about 10 nm. We drop casted and dried the prepared Ag NPs on a glass substrate for 6 cycles, then achieved absorption spectrum, which is shown in Fig. 2.b. The plasmonic peak relating to the Ag NPs is observed at 400 nm. Fig. 2.c presents the TEM image of the prepared rGO sheets. The Raman spectroscopy result of the rGO sheets is shown in Fig. 2.d, where the typical trace of rGO sheets at 1312 $cm^{-1}$ and 1580 $cm^{-1}$ are shown by arrows, corresponding to D band and G band, respectively [24]. It is well established that G band is attributed to the size of $sp^2$ carbon-type

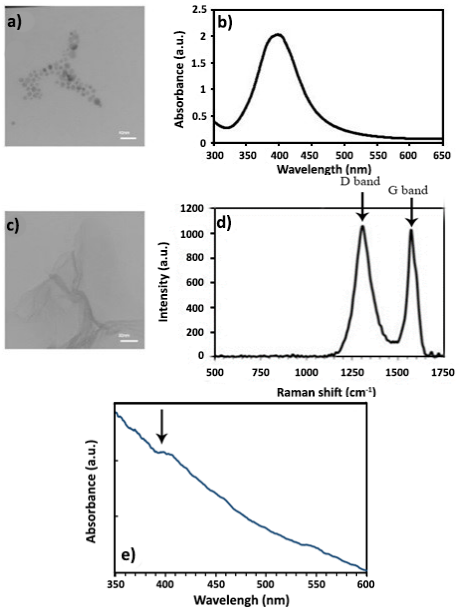


Fig. 2. (a) TEM image and (b) UV-Vis spectroscopy result of the synthesized Ag NPs. (c) TEM image and (d) Raman spectroscopy result of the prepared rGO sheets. (e) Absorption spectrum of the prepared Ag NPs/rGO heterostructure.

domains, while the D band refers to the structural imperfections in the hexagonal graphitic layers, including hydroxyl or epoxide groups in rGO sheets [24]. Fig. 2.e shows the absorption spectrum of rGO/Ag NPs heterostructure, where the absorption peak of Ag NPs at about 400 nm is detectable through the rGO absorption spectrum and is shown by an arrow. Fig. 3.a and Fig. 3.b display the measured short circuit current ($I_{SC}$) and open circuit voltage ($V_{OC}$) for a bare TENG with PDMS thickness of 20µm before coating Ag NPs. In Fig. 3.c, effect of adding Ag NPs on $V_{OC}$ of the TENG is studied. An enhanced open circuit peak-to-peak voltage is observed, by a factor of about 5 in comparison

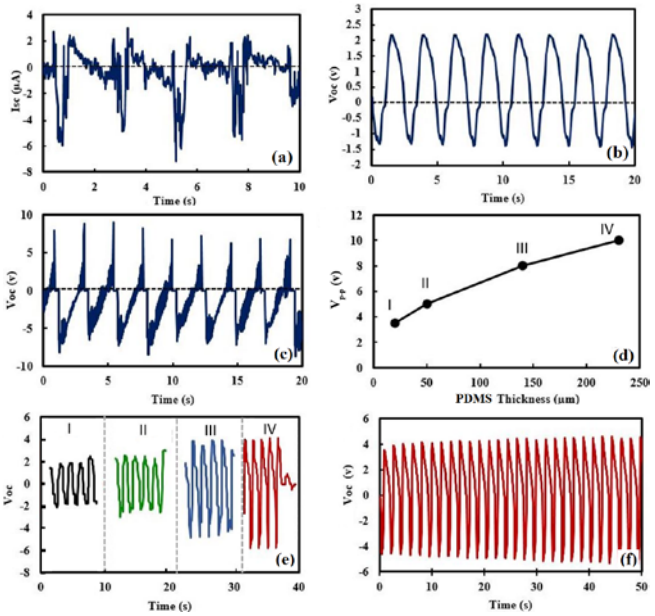


Fig. 3 (a) $I_{SC}$ and (b) $V_{OC}$ of the bare TENG, before coating Ag NPs. (c) The enhanced $V_{OC}$ of the TENG after coating Ag NPs. (d) Open circuit peak-to-peak voltage versus PDMS thickness, and (e) the $V_{OC}$ signals corresponding to different PDMS thicknesses. (f) $V_{OC}$ signal relating to continuous operating cycles.

with the bare sample (Fig. 3.b). This enhancement is attributed to the increased effective area of the contact surfaces in the presence of nanoparticles [25]. Fig. 3.d highlights the impact of varying PDMS thickness ($t_{PDMS}$) on the output open circuit peak-to-peak voltage ($V_{p-p}$) of the bare TENGs without Ag NPs. It can be observed that increasing $t_{PDMS}$ from 20µm to 230µm increases the open circuit peak-to-peak voltage from 3.5V to 10V. This observation can be attributed to the modulation of electrostatic induction by changing thickness of the PDMS layer, while tribo charges on its surface do not change. In other words, a fixed amount of generated tribo charges causes higher (lower) potential difference across a capacitor with lower (higher) capacity, for the case of thicker (thinner) PDMS layer. This observation is in agreement with the previous theoretical studies of Niu [26]. Fig. 3.e shows the output $V_{OC}$ signals, corresponding to different $t_{PDMS}$ values, investigated in part (d). Fig. 3.f displays $V_{OC}$ signal of the bare TENG with $t_{PDMS}$=230µm, in response to continuous pressing/releasing cycles, revealing an acceptable stability for the fabricated TENG. At the next stage, we present the fabricated self-powered UV-detector, based on rGO/Ag NPs heterostructure. First we investigate the photoresponse ($\Delta G/G_0$) of the rGO/Ag NPs layer (Fig. 4.a) in response to a Sun-Kraft UV lamp, revealing an enhancement factor of 2.6, comparing with the pristine rGO

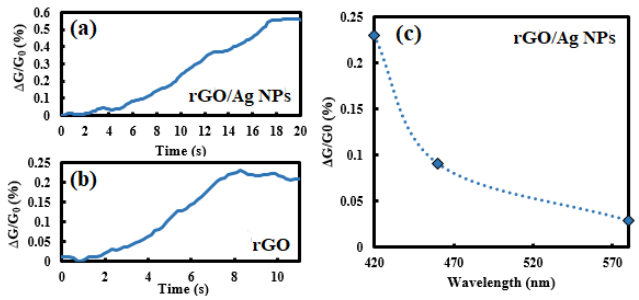


Fig. 4. Photoresponse of (a) rGO/Ag NPs, and (b) rGO layers to Sun-Kraft UV source. (c) Photoconductive sensitivity of rGO/Ag NPs layer in response to different visible wavelengths.

This article has been accepted for publication in a future issue of this journal, but has not been fully edited. Content may change prior to final publication. Citation information: DOI 10.1109/LED.2018.2854733, IEEE Electron Device Letters

layer (Fig. 4.b). This improved photoresponse is believed to be related to the excitement of localized surface plasmons in Ag NPs that can result in a kind of plasmon-assisted photodesorption of residual oxygen groups from the surface of rGO sheets. Similarly, Tan et al. have previously proved that this photodesorption effect in rGO/Ag NPs heterostructures dominates the ordinary photogeneration in the bare rGO sheets [27]. This plasmon-assisted desorption is believed to be originated from lowering of the adsorption strength and activation energy barrier for desorption, at the presence of an external electric field [28]. Moreover, Fig. 4.c presents the photoconductive sensitivity of rGO/Ag NPs layer in response to different visible wavelengths, which agrees with the reduction of Ag NPs' absorption spectrum in visible range (Fig. 2.b). Here, we benefit from the plasmon-assisted enhanced UV-response of rGO/Ag NPs heterostructure for realizing self-powered UV-detector. For this purpose, we incorporate the rGO/Ag NPs heterostructure as an UV-sensitive photoconductor in the configuration of fabricated TENG. Fig. 5.a indicates the applied UV-sensitive configuration, in which external force is exerted on the top steel plate and UV source is exposed from the bottom. Samples with 20μm-thick PDMS layers are investigated and a Sun-Kraft UV lamp (model A-1) has been utilized as the source. As depicted in Fig. 5.a, we have electrically connected the top steel electrode to the rGO/Ag NPs layer in the UV sensing structure in order to effectively incorporate the rGO/Ag NPs photoresistor in electrical configuration of the fabricated TENG. Fig. 5.b exhibits the response of the investigated UV-sensitive TENG based on rGO/Ag NPs, to UV illumination. As shown in this figure, the observed open circuit peak-to-peak voltage is near 2.5V before UV-illumination, however it is reduced to about 1.25V when illuminated, and returns to the initial value by turning the UV source off. The incident light power is about 500μW/cm$^2$ in this experiment. Fig. 5.c manifests a simplified equivalent circuit model for the presented UV-sensitive TENG, in which $c_1$ and $c_2$ represent the capacitances between the rGO/Ag NPs layer with the top steel electrode and bottom ITO layer, respectively. The capacitive value of $c_1$ varies during the pressing/releasing cycles, while $c_2$ is a fixed capacitor. The photoresistor ($R_{ph}$) represents the UV-sensitive rGO/Ag NPs layer which plays as a shunt resistance for $c_1$. The output $V_{OC}$ is measured between the top steel electrode and the bottom ITO electrode, as shown in Fig. 5.a. Regarding the equivalent circuit in dark condition, a high shunt resistance results in the typical operation of the TENG as discussed in the Fabrication Process and Operation Principle section. However, when the sample is exposed to UV illumination, the reduced shunt resistance causes the tribo charges on rGO layer to discharge and $V_{OC}$ to decrease. Fig. 5.d illustrates the open circuit sensitivity ($=\Delta V_{p\text{-}p}/V_{p\text{-}p}$), in response to different incident light powers of the utilized Sun-Kraft UV lamp. It can be observed that increasing incident illumination power from 70μW/cm$^2$ to 500μW/cm$^2$ results in raising sensitivity from rom 10% to about 50%. To elaborate the visible response of the realized self-powered UV detector, the open circuit sensitivity has been measured in response to three different monochromatic visible sources with the same illumination powers. Fig. 5.e illustrates the photoresponse spectrum, confirming that the output sensitivity decreases when the incident wavelength increases that is consistent with the plasmonic absorption spectra of Ag NPs (Fig. 2.b). Benefiting from the plasmonic behavior of Ag NPs in this approach, we have realized a high sensitive self-powered UV detector, which is blind to Deep-UV and visible range, and possesses UV-selective photoresponse. Furthermore, tunability of the UV-sensitive range of this detector may be achieved by controlling size distribution of Ag NPs, which can be proposed as another potential for the presented UV detector.

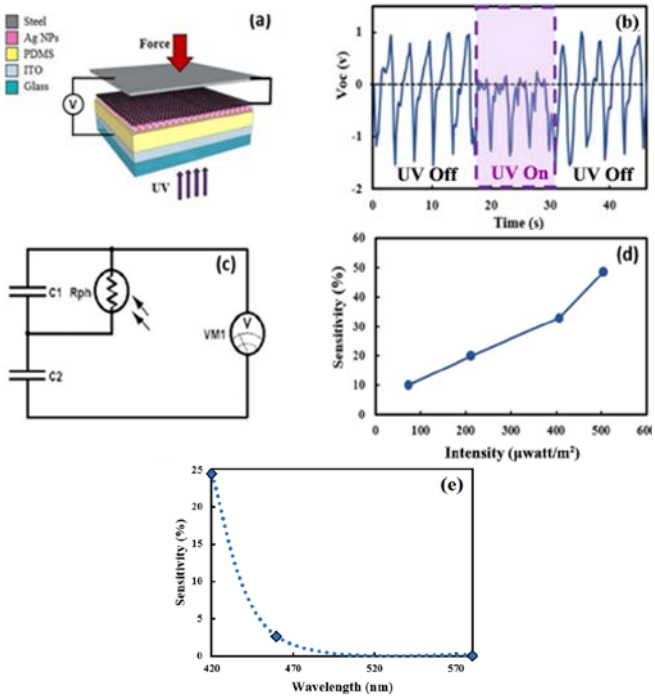


Fig. 5. (a) The applied UV-sensitive TENG configuration. (b) The measured $V_{OC}$ in response to Sun-Kraft UV source. (c) The equivalent circuit model for the fabricated self-powered UV detector. (d) UV-response of $V_{OC}$ versus different illumination powers. (e) Output sensitivity versus different incident wavelengths.

## IV. Conclusion

We reported a plasmonic self-powered UV detector based on TENG, by taking advantage of rGO/Ag NPs heterostructure as the UV-sensitive layer. It is proved that the rGO/Ag NPs layer shows a plasmon-assisted improved photoresponse to UV-illumination. Presence of Ag NPs improves the output $V_{OC}$ of the triboelectric nanogenerator by a factor of about 5, which can be related to the enhanced surface area of the contacting electrodes. When exposed to UV illumination with light power of 500 μW/cm$^2$, the output $V_{OC}$ of the fabricated triboelectric nanogenerator responds with a sensitivity ($\Delta V_{p\text{-}p}/V_{p\text{-}p}$) of about 50%. In summary, we have achieved a high sensitive and UV-selective self-powered plasmonic detector based on TENGs, for the first time.

## Acknowledgments

The authors acknowledge the partial financial support of the Iran National Science Foundation (INSF) 95821267, and the financial support from Tarbait Modares University, through grant #IG-39703.

## REFERENCES


[1] Z. L. Wang, J. Song, "Piezoelectric Nanogenerators Based on Zinc Oxide Nanowire Arrays," Science, 312, 242-246, 2006. DOI: 10.1126/science.1124005

[2] M.E. Kiziroglou, C. He, E. M. Yeatman, "Flexible substrate electrostatic energy harvester," Electron Lett. 46(2), 166-7, 2010. DOI: 10.1049/el.2010.2462

[3] E. Modaresinezhad, S. Darbari, "Realization of a room-temperature/self-powered humidity sensor, based on ZnO nanosheets," Sens. and Act. B: Chem. 237, 358-366, 2016. DOI: 10.1016/j.snb.2016.06.097

[4] F. R. Fan, Z. Q. Tian, Z. L. Wang, "Flexible triboelectric generator," Nano Energy 1, 328–334, 2012. DOI: 10.1016/j.nanoen.2012.01.004

[5] K. Parida, V. Kumar, W. Jiangxin, V. Bhavanasi, R. Bendi, P. S. Lee, "Highly Transparent, Stretchable, and Self-Healing Ionic-Skin Triboelectric Nanogenerators for Energy Harvesting and Touch Applications," Adv. Mat. 1702181-8, 2017. DOI: 10.1002/adma.201702181

[6] A. Li, Y. Zi, H. Guo, Z.L. Wang, F.M. Fernandez, "Triboelectric nanogenerators for sensitive nano-coulomb molecular mass spectrometry," Nature Nanotech. 12, 481-7, 2017. DOI: 10.1038/nnano.2017.17

[7] M. Javadi, A. Heidari, S. Darbari, "Realization of enhanced sound-driven CNT-based triboelectric nanogenerator, utilizing sonic array configuration," Curr. Appl. Phys. 18, 361-368, 2018. DOI: 10.1016/j.cap.2018.01.018

[8] M. Taghavi, B. M. A. Sadeghi, L. Beccai, V. Mattoli, "Triboelectric-based harvesting of gas flow energy and powerless sensing applications," Appl. Sur. Sci. 323, 82-87, 2014. DOI: 10.1016/j.apsusc.2014.07.025

[9] M. Taghavi, A. Sadeghi, A. Mondini, B. Mazzolai, L. Beccai, V. Mattoli, "Triboelectric smart machine elements and self-powered encoder," Nano Energy 13, 92-102, 2015. DOI: 10.1016/j.nanoen.2015.02.011

[10] M. Taghavi, L. Beccai, "A contact-key triboelectric nanogenerator: Theoretical and experimental study on motion speed influence," Nano Energy 18, 283-292, 2015. DOI: 10.1016/j.nanoen.2015.10.019

[11] M. Taghavi, V. Mattoli, A. Sadeghi, B. Mazzolai, L. Beccai, "A Novel Soft Metal-Polymer Composite for Multidirectional Pressure Energy Harvesting," Adv. En. Mat. 2014; 4: 1400024. DOI: 10.1002/aenm.201400024

[12] Y. Xie, S. Wang, S. Niu, L. Lin, Q. Jing, J. Yang, Z. Wu, Z. L. Wang, "Grating-Structured Freestanding Triboelectric-Layer Nanogenerator for Harvesting Mechanical Energy at 85% Total Conversion Efficiency, " Adv Mat. 26(38), 6599–607, 2014. DOI: 10.1002/adma.201402428

[13] X. S. Zhang, M. D. Han, B. Meng, H. X. Zhang, "High performance triboelectric nanogenerators based on large-scale mass-fabrication technologies," Nano Energy, 11(0), 304-22, 2015. DOI: 10.1016/j.nanoen.2014.11.012

[14] S. Wang, L. Lin, Z. L. Wang, "Triboelectric nanogenerators as self-powered active sensors," Nano Energy, 11, 436-62, 2015. DOI: 10.1016/j.nanoen.2014.10.034

[15] F. R. Fan, L. Lin, G. Zhu, W. Z. Wu, R. Zhang, Z. L. Wang, "Transparent Triboelectric Nanogenerators and Self-Powered Pressure Sensors Based on Micropatterned Plastic Films," Nano Lett., 12(6), 3109–14, 2012. DOI: 10.1021/nl300988z

[16] G. Zhu, W. Q. Yang, T. J. Zhang, Q. S. Jing, J. Chen, Y. S. Zhou, P. Bai, Z. L. Wang, "Self-Powered, Ultrasensitive, Flexible Tactile Sensors Based on Contact Electrification," Nano Lett., 14(6), 3208–13, 2014. DOI: 10.1021/nl5005652

[17] H. Yu, X. He, W. Ding, Y. Hu, D. Yang, S. Lu, C. Wu, H. Zou, R. Liu, C. Lu, Z. L. Wang, "A Self-Powered Dynamic Displacement Monitoring System Based on Triboelectric Accelerometer," 1700565, 2017. DOI: 10.1002/aenm.201700565

[18] Z. H. Lin, G. Cheng, Y. Yang, Y. S. Zhou, S. Lee, Z. L. Wang, "Triboelectric Nanogenerator as an Active UV Photodetector," Adv. Funct. Mater., 24, 2810–6, 2014. DOI: 10.1002/adfm.201302838

[19] L. Su, Z. X. Zhao, H. Y. Li, J. Yuan, Z. L. Wang, G. Z. Cao, G. Zhu, "High-Performance Organolead Halide Perovskite-Based Self-Powered Triboelectric Photodetector," ACS Nano., 9(11), 11310–6, 2015. DOI: 10.1021/acsnano.5b04995

[20] L. Su, H. Y. Li, Y. Wang, S. Y. Kuang, Z. L. Wang, "Coupling of photoelectric and triboelectric effects as an effective approach for PZT-based high-performance self-powered ultraviolet photodetector," Nano Energy, 31, 264–9, 2017. DOI: 10.1016/j.nanoen.2016.11.019

[21] L. Mulfinger, S. D. Solomon, M. Bahadory, A. V. Jeyarajasingam, S. A. Rutkowsky, C. Boritz, "Synthesis and Study of Silver Nanoparticles, " J. Chem. Educ., 84(2), 322-5, 2007. DOI: 10.1021/ed084p322

[22] J. Chen, B. Yao, C. Li, G. Shi, "An improved Hummers method for eco-friendly synthesis of graphene oxide," Carbon 64, 225-229, 2013. DOI: 10.1016/j.carbon.2013.07.055

[23] N. Kaur, J. Bahadur, V. Panwar, P. Singh, K. Rathi, K. Pal, "Effective energy harvesting from a single electrode based triboelectric nanogenerator," Sci. Rep., 6(38835), 2016. DOI: 10.1038/srep38835

[24] D. Yang, A. Velamakanni, G. Bozoklu, S. Park, M. Stoller, R. D. Piner, S. Stankovich, I. Jung, D. A. Field, C. A. Ventrice Jr., R. S. Ruoff. "Chemical analysis of graphene oxide films after heat and chemical treatments by X-ray photoelectron and Micro-Raman spectroscopy," Carbon, 47(1), 145-52, 2009. DOI: 10.1016/j.carbon.2008.09.045

[25] G. Zhu, Z. H. Lin, Q. Jing, P. Bai, C. Pan, Y. Yang, Y. Zhou, Z. L., "Wang Toward Large-Scale Energy Harvesting by a Nanoparticle-Enhanced Triboelectric Nanogenerator," Nano Lett. 13(2), 847-53, 2013. DOI: 10.1021/nl4001053

[26] S. Niu, S. Wang, L. Lin, Y. Liu, Y. S. Zhou, Y. Hua, Z.L.Wang, "Theoretical study of contact-mode triboelectric nanogenerators as an effective power source, "Energy Environ Sci. 6, 3576-83, 2013.DOI:10.1039/C3EE42571A

[27] W.C. Tan, M. Hofmann, Y-P. Hsieh, M.L. Lu, Y. F. Chen, "A graphene-based surface plasmon sensor," Nano Res., 5, 695-702, 2012. DOI: 10.1007/s12274-012-0253-y

[28] H. Akpati, P. Nordlander, L. Lou, P. Avouris, "The effects of an external electric field on the adatom-surface bond: H and Al adsorbed on Si (111), " Sur. Sci., 372(1-3), 9-20, 1997. DOI: 10.1016/S0039-6028(96)01117-X